PCCP

PAPER

View Article Online
View Journal | View Issue

Crystallization of zirconia based thin films

Cite this: *Phys. Chem. Chem. Phys.*, 2015, **17**, 18613

D. Stender,[a] R. Frison,[b] K. Conder,[b] J. L. M. Rupp,[c] B. Scherrer,[d] J. M. Martynczuk,†[e] L. J. Gauckler,[d] C. W. Schneider,[a] T. Lippert*[a] and A. Wokaun[a]

Published on 23 June 2015. Downloaded by MIT Library on 6/18/2019 3:35:39 PM.

Received 6th May 2015,
Accepted 19th June 2015

DOI: 10.1039/c5cp02631h

www.rsc.org/pccp

The crystallization kinetics of amorphous 3 and 8 mol% yttria stabilized zirconia (3YSZ and 8YSZ) thin films grown by pulsed laser deposition (PLD), spray pyrolysis and dc-magnetron sputtering are explored. The deposited films were heat treated up to 1000 °C *ex situ* and *in situ* in an X-ray diffractometer. A minimum temperature of 275 °C was determined at which as-deposited amorphous PLD grown 3YSZ films fully crystallize within five hours. Above 325 °C these films transform nearly instantaneously with a high degree of micro-strain when crystallized below 500 °C. In these films the t″ phase crystallizes which transforms at $T > 600$ °C to the t′ phase upon relaxation of the micro-strain. Furthermore, the crystallization of 8YSZ thin films grown by PLD, spray pyrolysis and dc-sputtering are characterized by *in situ* XRD measurements. At a constant heating rate of 2.4 K min^{-1} crystallization is accomplished after reaching 800 °C, while PLD grown thin films were completely crystallized already at *ca.* 300 °C.

Introduction

Thin films of yttria stabilized zirconia (YSZ) are the most commonly used electrolyte membranes for micro solid oxide fuel cells (μSOFCs).[1–10] These membranes have to fulfil several requirements: (1) they have to be thin enough (<1 μm) to reduce ohmic losses to values below 0.15 Ω cm^{-2} at temperatures below 500 °C.[6,11–13] (2) Full crystallinity of the metal oxide electrolytes has to be assured. Ongoing crystallization processes and amorphous residues are disadvantageous for ionic diffusion in a transforming "metastable" lattice.[14] In addition, etching resistances in μSOFC processing depend strongly on the degree of crystallinity.[15] (3) Gas tightness and thermal–mechanical stability are mandatory.[16] Thermal stress may result from a mismatch of the thermal expansion coefficients of adjacent materials as well as from shrinkage due to on-going crystallization and hence volume change of the YSZ films upon further annealing during operation. This stress is typically tensile. One possible way to avoid thermally induced stresses is to deposit films by PLD at temperatures as low as possible in order to use atomic peening to introduce compressive stresses in order to compensate the thermal expansion mismatch stresses as well as those related to crystallization.[7,17–19] The PLD deposition conditions can lead to fully crystalline thin films with a columnar microstructure with column widths of a few tens of nanometres at temperatures as low as 600 °C.[20,21]

Alternatively, the PLD deposition of YSZ at ambient temperature results in dense and amorphous thin films that can be crystallized during a post deposition annealing. A comprehensive study on the deposition and crystallization of 8YSZ (8 mol% Y_2O_3 doping) thin films by PLD at ambient temperature was published by Heiroth *et al.*[22] The authors report that the minimum crystallization temperature is around 250 °C whereby fully crystalline films can be obtained after an isothermal hold for 15 h. At 350 °C the 8YSZ films crystallized almost instantaneously.

In recent years an interest in lower doped YSZ also emerged *e.g.* 3YSZ (3 mol% Y_2O_3 doping with a tetragonal crystalline structure) due to its higher fracture toughness imparted by a transformation toughening process as compared to 8YSZ, which stabilizes in the cubic phase and has no possibility to compensate for applied stress.[23–25] It will therefore break more readily as compared to 3YSZ. The higher toughness is explained by a martensitic phase transition from a tetragonal to monoclinic crystal structure which is accompanied by a ≈4% volume increase.[26] With respect to electrical properties, 3YSZ has a similar ionic conductivity as 8YSZ at temperatures around 500 °C.[20,23] Thus, it is of general interest to compare the crystallization process of 3YSZ with 8YSZ, which is the main aim of this work. Especially for PLD grown oxides only a few studies about the amorphous to crystalline phase transitions have been performed.[22,27]

For the purpose of comparison of the crystallization of initially amorphous thin films, the method of time–temperature-transformation (TTT) diagrams was recently proposed and

[a] Paul Scherrer Institut, Research Department General Energy, 5232 Villigen, Switzerland. E-mail: thomas.lippert@psi.ch
[b] Paul Scherrer Institut, Laboratory for Developments and Methods, 5232 Villigen, Switzerland
[c] ETH Zurich, Electrochemical Materials, 8093 Zurich, Switzerland
[d] ETH Zurich, Nonmetallic Inorganic Materials, 8093 Zurich, Switzerland
[e] ETH Zurich, Electron Microscopy ETH Zurich, 8093 Zurich, Switzerland
† Present address: KoinaSoft GmbH, CH-8048 Zurich, Switzerland.

Published on 23 June 2015. Downloaded by MIT Library on 6/18/2019 3:35:39 PM.

applied for gadolinia doped and undoped ceria thins films grown by spray pyrolysis (SP).[28] TTT diagrams are often used to describe the phase transformations of glass ceramics, metals and metallic glasses.[29–31] It is expected, that the crystallization temperatures of the PLD grown thin films are much lower than for SP grown films as they contain no organic residues and were deposited at higher deposition kinetic energies of the plasma species. Therefore, 8YSZ thin films were also prepared by spray pyrolysis and direct current (dc) magnetron sputtering to compare their crystallization process with PLD grown films. These results may help in choosing the appropriate preparation method for specific demands.

Experimental

A series of amorphous 3YSZ thin films were deposited on c-cut sapphire single crystalline substrates by PLD at ambient temperature. The cylindrical target was fabricated of 3 mol% yttria doped zirconia powders (Tosoh Corp., Japan) by uniaxial pressing at 4 kbar and subsequent sintering for 4 h at 1400 °C to full density and a grain size of 350 nm. The ablation was achieved with a Compex 301 KrF Excimer Laser (Lambda Physik) at a wavelength of 248 nm. To reach a fluence of 2.0 J cm^{-2} the laser beam was reduced by a lens to a rectangular area of 1.3 mm^2. The sapphire single crystalline substrate was placed on a rotating sample holder 4 cm from the revolving target. A total of 11 000 pulses at a repetition rate of 5 Hz were used, to obtain 140 $\pm$ 10 nm thin films as verified by a surface profilometer (Dektak 8, Veeco Inc.). For all depositions an oxygen atmosphere at a pressure of 1.6×10^{-2} mbar was applied in the PLD chamber. Details on the fabrication of the PLD grown 8YSZ thin films can be found elsewhere.[22]

To compare the crystallization kinetics as a function of the deposition method, 8YSZ thin films were also grown by spray pyrolysis and dc-magnetron sputtering. The dc-sputtered films were grown at room temperature at an oxygen background pressure of 1.2×10^{-2} mbar. The target (84 mol% zirconium and 16 mol% yttrium) was sputtered for 110 min at a power of 200 W to obtain 200 nm thick 8YSZ thin films. Details on the deposition of the SP grown films and references therein can be found elsewhere.[32] The SP grown films were cooled to ambient temperature directly after the deposition at 370 °C without any annealing step to avoid crystallization prior the measurements.

The *ex situ* annealing of these thin films up to 1000 °C was done in a tube furnace. The heating rate was set to 5 K min^{-1} and the final temperature was kept for 20 h before the samples were cooled down to room temperature at the same rate. *In situ* annealing was performed in a D500 X-ray diffractometer (XRD) from Bruker–Siemens (Germany) with the high temperature attachment HTK10 from Anton Paar (Austria). Two different heating programs were used: (1) for isothermal dwells at temperatures from 250 °C to 325 °C a heating rate of 30 K min^{-1} was applied to minimize the influence of the heating history. (2) A slow heating rate of 2.4 K min^{-1} followed by an isothermal dwell at 800 °C. This enables to observe changes in the diffraction pattern depending on the actual present temperatures.

To reduce the time between two acquisitions to less than one minute the scan range was set from 29° to 31° with a step size of 0.02° and 0.5 s per step. The (101) reflex of the tetragonal structure was chosen for observation because it has the highest intensity. For the calculation of the peak intensity from the diffraction pattern a baseline subtraction was performed with a subsequent integration of the peak area.

Additional information about the crystal symmetry was obtained using μ-Raman microscopy (LabRAM Series, Horiba Jobin Yvon). A He–Ne laser at 632.8 nm is focused to an active interaction volume of ≈ 1 μm^3. To distinguish the overlapping sapphire and YSZ Raman mode at ≈ 640 cm^{-1} a special geometry was used. The samples were placed on their edge and consecutive scans were performed while moving the specimen along a lateral axis. Thereby, some scans were solely performed in air, on the film, and on the substrate. The scan with the highest intensity of film peaks was chosen, followed by a subtraction of a Raman spectrum of the substrate of this scan series multiplied with an arbitrary factor selected to eliminate the strong sapphire peak at *ca.* 418 cm^{-1}. Although it cannot be completely ruled out that there is still a small but finite substrate contribution to the final spectrum, the results look reasonable and are sufficient to deduce peak shifts with increasing annealing temperatures (see Results section). Additionally, all spectra were calibrated for the strong sapphire Raman mode at ≈ 418 cm^{-1}.[33]

The surface micro-structures of these films were characterized by atomic force microscopy (AFM). The surfaces of the samples were scanned with a Nanoscope IIIa SPM (Veeco) in tapping mode over an area of 10×10 μm^2 with a resolution of 512×512 pixels. The raw images were analysed with the WSxM software.[34] In addition scanning electron microscopy (SEM) was performed on a Zeiss Supra VP55 FE-SEM. The surface structure was imaged with the SE2 detector for back scattered electrons. Prior to the SEM measurements the samples were coated with a 10 nm chromium layer in order to avoid charging. Transmission electron microscopy (FEI Tecnai F-30) with an accelerating voltage of 300 kV and post-column CCD camera was applied to obtain bright-field and dark-field transmission electron micro-graphs (BF and DFTEM) to investigate the cross sections of the samples. For this purpose, slices were cut out of the samples by a focused ion beam (FIB) with a dual beam FIB/SEM (Zeiss NVision40) equipped with a gallium liquid metal ion source, a gas injection system and a micro-manipulator MM3A from Kleindiek. A layer of amorphous carbon was deposited first with the e-beam and then with the ion beam on the surface to protect the thin film before cutting trenches from both sides with 13 and 3 nA at 30 kV. After the lift-out was performed the lamellae were polished to ion transparency with currents down to 10 pA at 30 kV. The amorphization was diminished by low kV showering for several seconds at 5 kV.

Results and discussion

Analysis of the crystal symmetry

The diffraction pattern of *ex situ* annealed 3YSZ thin films between 250 °C and 1000 °C are shown in Fig. 1. A sample

 This journal is © the Owner Societies 2015

Published on 23 June 2015. Downloaded by MIT Library on 6/18/2019 3:35:39 PM.

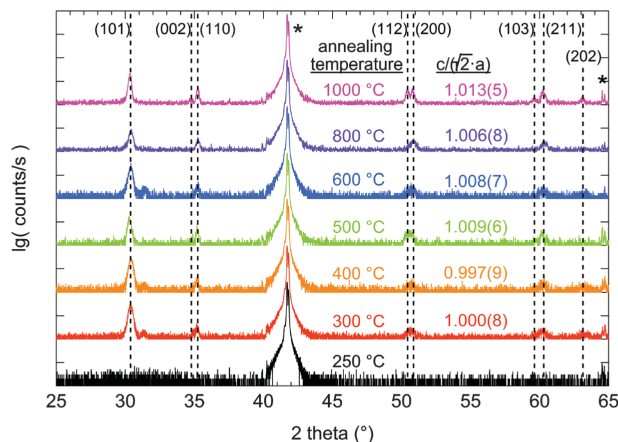

Fig. 1 Diffraction pattern of *ex situ* annealed 3YSZ thin films grown by PLD obtained in $\Theta/2\Theta$ geometry. The dashed lines indicate the theoretically observable reflexes of the tetragonal zirconia lattice. Substrate reflexes are marked by an asterisk. The origin of the small peak at ≈31.4° is not clear at present, but may originate from a small fraction of monoclinic YSZ(111).

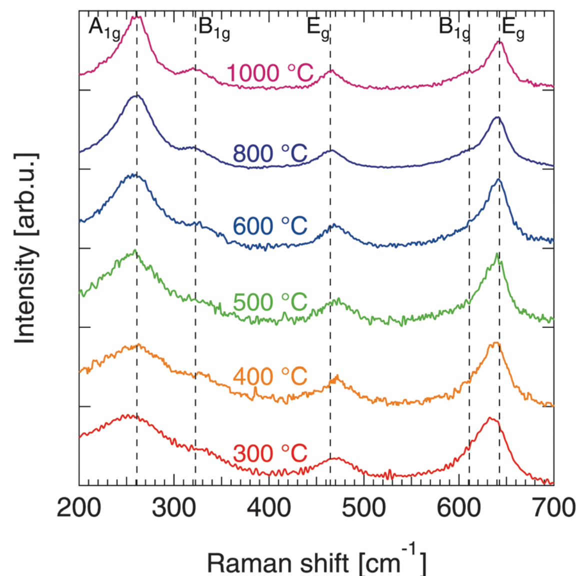

Fig. 2 Raman spectra of *ex situ* annealed 3YSZ thin films grown by PLD. Dashed lines mark the Raman active phonon frequencies of tetragonal zirconia.[39]

which was annealed at 250 °C did not show any 3YSZ diffraction reflexes, *i.e.* no crystallization occurred up to this temperature. All shown XRD patterns were corrected for displacement offsets by utilizing the (0006) sapphire peak at 41.7.[35] The positions of the expected reflexes of 3YSZ polycrystalline material are indicated by dashed lines. The relative peak intensities reflect well the measured intensity ratios of polycrystalline powder (*e.g.* see PDF No. 01-089-9068). Thus, no preferential orientation of the crystallites were observed. The volume of the unit cell shows a small increase of 0.5 ± 0.7% from 300 °C to 1000 °C which is expected from crystallographic data on cubic (*e.g.* see PDF No. 030-1468) and tetragonal YSZ. Additionally, the calculated ratios of $c/(\sqrt{2}\cdot a)$ are given in Fig. 1 for each of the samples, where a ratio of one is equivalent to the cubic symmetry (a and c are the lattice parameters of the assumed tetragonal lattice) with c changing from 0.509 nm at 300 °C to 0.51514 nm at 1000 °C. Although the uncertainties for each value is considerable, a tendency from cubic towards a 'more tetragonal' structure with increasing annealing temperature is noted. A more detailed characterization of the phases follows from the Raman results.

A narrowing of the diffraction peaks, *i.e.* smaller full widths at half maximum (FWHM) is observed for films annealed at higher temperatures. *E.g.* the (101)-peak for a film annealed at 300 °C and 1000 °C narrows from 0.34° to 0.20° (including instrumental broadening). This effect is usually attributed to two possible origins: first, grain growth takes place at higher temperatures and the grain size can be determined with the Scherrer equation.[36] Second, micro-strain leads to a broadening of the FWHM.[37,38] Since the average grain size is limited by the annealing temperature the decrease in FWHM is most probably related to a release of strain at higher annealing temperatures. Support for this hypothesis will be given next in the Raman and micro-structural analysis.

To gain further insight into the crystal structure and local near-order, Raman spectra of the samples are presented in Fig. 2. All samples show typical Raman spectra of tetragonal YSZ with five Raman active modes between 200 and 700 cm^{-1}.[2,39] The tetragonality is not a contradiction to the XRD results since X-rays probe the lattice plane spacing of the heavy zirconium and yttrium ions only which looks like a cubic phase. This t″ metaphase exhibits an axial ratio of unity as expected for a cubic cell in contrast to the tetragonal phase found also for pure ZrO_2 (t or t′) where the tetragonal symmetry is derived from the elongation of the c-axis and shrinkage of the a-axis. The tetragonal symmetry of the t″ metaphase, however, is induced by oxygen dislocations along the c-axis.[40,41] Distinct changes of the spectral peak positions and their FWHM with increasing annealing temperature are clearly visible. All modes show mainly a Lorentzian shape with a slight asymmetry. While the peak positions of the modes around 320 cm^{-1}, 610 cm^{-1} and 640 cm^{-1} (B_{1g}, E_g and B_{1g} modes) are subject to uncertainties due to overlapping with adjacent peaks and a possible residue from the sapphire substrate, the values for the modes around 260 cm^{-1} and 460 cm^{-1} (A_{1g} and E_g mode) can be well determined. Several changes in the Raman spectra for different annealing temperatures are observed: a red shift of ≈5 cm^{-1} is found for the A_{1g} mode and a blue shift for the E_g mode of approximately the same magnitude. The A_{1g} mode is broadened by ≈40 cm^{-1} to ≈80 cm^{-1} for the samples annealed at 1000 °C and 300 °C, respectively. The relative intensity of the A_{1g} mode compared to the B_{1g} and E_g modes above 600 cm^{-1} increases for higher temperatures. In the literature these three observations are related to the release of compressive stress.[42,43]

As pointed out in ref. 42 and 43 an increase of compressive stress results in an increasingly cubic-like crystal structure ($c/(\sqrt{2}\cdot a) \rightarrow 1$). This confirms the results from the XRD measurements where a ratio of $c/(\sqrt{2}\cdot a) \approx 1$ was found for annealing temperatures of 300 °C and 400 °C corresponding to a cubic symmetry of the cation sublattice. This lowering of symmetry

with increased annealing temperature coincides well with the results from[22] where 8YSZ thin films, crystallized at 300 °C, showed a complete cubic phase even in the Raman spectrum, while samples annealed at > 500 °C show the t″ phase. Hence, a relaxation of the thin film, which is only possible at higher temperatures, increases the 'tetragonality' of YSZ in general.

Analysis of the crystallization kinetics

The time evolution of the integrated *in situ* measured XRD intensity of the (101)-reflex for three PLD 3YSZ thin films annealed at 275 °C, 300 °C and 325 °C are shown in Fig. 3. For the purpose of comparability the origin of the time scale was set to the moment when the final temperature was reached. As stated in the Experimental section, a fast heating with 30 K min^{-1} was used and therefore it can be assumed, that the crystallization starts at this point in time. Like for the *ex situ* annealed samples no crystallization was detected for a sample held at 250 °C up to 100 h. In contrast, a sample annealed at 350 °C was already crystallized during the acquisition of the first data point. At the in-between temperatures an exponential increase of annealing time was observed.

The description of the nucleation and grain growth processes is generally performed *via* the Johnson–Mehl–Avrami–Kolmogorov (JMAK) model.[44–47] Within this description of a phase transformation the crystallized volume fraction $x(t)$ (equivalent to the normalized integrated XRD peak intensity) is $x(t) = 1 - \exp(kt^n)$, where k is a temperature dependent rate constant and n the Avrami exponent. A least squares fit, using this equation, was performed for each of the three samples. The fit parameters are shown in Table 1

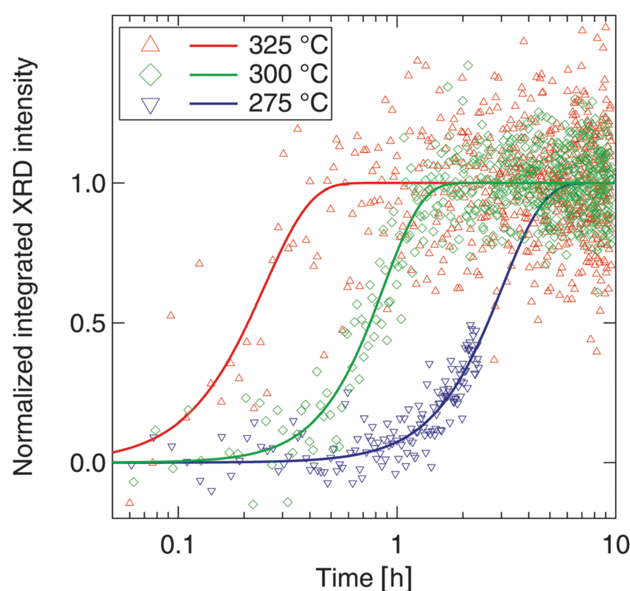

Fig. 3 Time evolution of the integrated XRD intensity of the (101) diffraction peak for isothermal dwells of PLD grown 3YSZ films at 275 °C, 300 °C and 325 °C. The origin of the time scale is set to the moment, when the final temperature was reached. The measurement at 275 °C was interrupted by an instrument error and the normalization was done with a measurement after the crystallization had finished. The fits for each measurement are based on the JMAK model.

Table 1 Parameters of the JMAK fits for the PLD grown and *in situ* annealed 3YSZ thin films at the given temperatures are presented. For comparison results for 8YSZ thin films are included[22]

	3YSZ		8YSZ[22]	
	n	$k[s^n]$	n	$k[s^n]$
250 °C	—	—	3.25	2.7×10^{-15}
275 °C	2.30	5.1×10^{-10}	2.92	8.4×10^{-12}
300 °C	2.47	2.3×10^{-9}	3.00	1.4×10^{-9}
325 °C	2.06	8.3×10^{-7}	1.76	1.6×10^{-4}

together with results for 8YSZ thin films.[22] Since k depends on n (n changes the unit of k), the k-values are not directly comparable for different values of n. This is not the case for the Avrami exponents which show distinct differences. In literature, the Avrami exponent is usually associated with the nucleation and the growth mode of the crystallites.[46,48] With a time constant number of nuclei, n equals the dimension of the growth, *e.g.* 2-dimensional growth results in $n = 2$ while a constant increase of nucleation centers additionally increases n by one. The Avrami exponents are around 3 for the 8YSZ thin films and close to 2 for the 3YSZ thin films. The only 8YSZ sample which shows a lower value was annealed at 325 °C. However, it is not clear at present why a value smaller than 2 occurs which would indicate a more two dimensional growth with a limited number of nucleation sites not observed in 8YSZ so far.

For 3YSZ and 8YSZ the films' microstructure was studied by different imaging methods to analyze whether this difference occurred due to a difference in the dimensionality of the crystallization. The AFM images of the surfaces of the 3YSZ thin films annealed at 275–325 °C are shown in Fig. 4a–c. The detailed micro-structure is best visible due to larger feature sizes for the sample annealed at 325 °C (Fig. 4b). Bright lines (additionally highlighted by some green lines in Fig. 4b) separate different structures in the micron range. Inside these structures, some kind of a central point (indicated by blue spots) is visible.

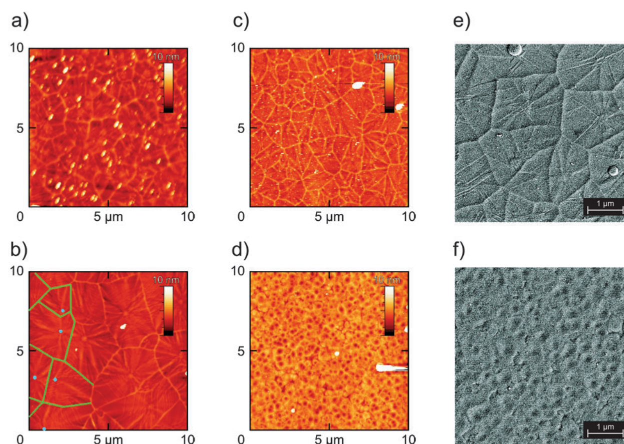

Fig. 4 AFM (a–d) and SEM (e and f) images of different PLD grown YSZ thin films: (a) 3YSZ annealed at 275 °C; (b) 3YSZ annealed at 325 °C; (c and e) 3YSZ annealed at 300 °C; (d and f) 8YSZ annealed at 300 °C. Some spots and lines illustrating the positions of crystallization centers and structural boarders are included in (b).

Published on 23 June 2015. Downloaded by MIT Library on 6/18/2019 3:35:39 PM.

Published on 23 June 2015. Downloaded by MIT Library on 6/18/2019 3:35:39 PM.

Again, the bright lines run in most cases directly in the middle between two of these central points. In addition, nearly all corners of the studied grain boundaries show angles of less than 180°. Considering crystallization processes, it is probable that these spots represent the origin of the crystallization (*i.e.* the nucleation centers) which proceeds until it encounters another ongoing crystallization. Although these observations are not always clearly distinguishable for the other two samples, they seem to be also present. An average feature size can be only roughly estimated due to the low statistics of the number of structures. For the 3YSZ film annealed at 300 °C this was done with the Lince software[49] and an average structure diameter of 0.9 μm was found. A similar value is found for the sample annealed at 275 °C, whereas it is approximately 2–3 μm for the thin film annealed at 325 °C. Furthermore, the observed structures seem to have an additional internal micro-structure. This could be related to the internal micro-strain. To confirm these observations, SEM scans of the samples annealed at 300 °C were taken (see Fig. 4e) verifying the grain size and structure as observed using AFM.

Based on these AFM and SEM studies it is not fully clear if the observed surface features indicate the growth of single grains or not. To clarify this issue cross sectional TEM imaging was used on the 3YSZ sample which was annealed at 300 °C. In Fig. 5a the bright field image of the 3YSZ thin film shows three regions of very different contrast: light, dark, light. The dark structure has a width of 830 nm and a height of 170 nm. Taking a selected area electron diffraction of this region verifies that this part of the 3YSZ film has single crystalline properties with one orientation only surrounded by two other crystallites with one, but a different orientation. The dark area in the BF image and the bright area in the DF image therefore shows crystallites with single crystalline properties with a cross sectional area of 830×170 nm^2. An aspect ratio of ~ 5 indicates that the grain growth proceeded mainly in two dimensions in agreement with the JMAK analysis. Along the same cross sectional cut, several large single grains as shown in Fig. 5 with a width of 0.4–2 μm where identified. It is therefore concluded, that the observed surface structures in Fig. 4c and e show the boundaries of single oriented grains which have a pronounced two-dimensional expansion.

These structures differ strongly from previous observations of crystallized 8YSZ thin films where typical structure sizes of ≈ 200 nm were found.[22] For this reason a 8YSZ thin film was prepared and annealed *ex situ* at 300 °C. The results of AFM and SEM measurements are shown in Fig. 4d and f. Both images confirm the previously reported results.[22] The density of nucleation centers seems to be much higher in 8YSZ films compared to 3YSZ films. Whether this is related to the PLD process, the target preparation, the powder from which the target is made, or the different doping concentrations is not clear yet. There might be a change in the surface energies between the differently doped materials which causes a change of the activation energy of critical nuclei.

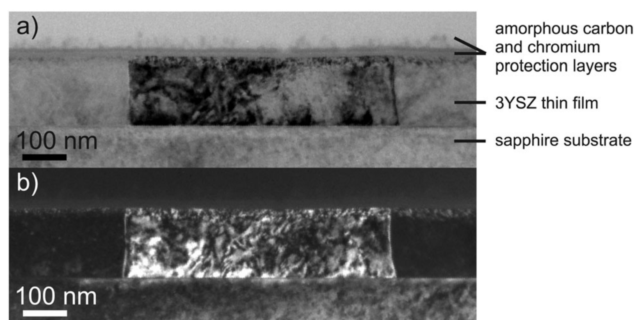

Fig. 5 Cross sectional bright field (a) and dark field (b) TEM images of a FIB cut slice of a 3YSZ thin film crystallized at 300 °C.

The observed structure sizes fit the results from the JMAK analysis well. For the 8YSZ thin films the grains' aspect ratios are close to one and therefore a 3-dimensional growth mode is reasonable. For 3YSZ the aspect ratios of the observed structures are larger than five, *i.e.* the main part of the crystallization proceeds in two dimensions only. This is most likely the reason for the lower Avrami exponents for 3YSZ compared to the 8YSZ films.

Comparison of different deposition techniques

The crystallization process of PLD grown YSZ films was analysed in the previous sections. These results are compared to those of YSZ thin films grown by other deposition processes to evaluate their performance depending on the annealing temperature and time. For this purpose 8YSZ thin films were grown by dc-magnetron sputtering and spray pyrolysis. In the case of the SP grown sample it is known, that temperatures of >500 °C are necessary to remove organic residues which is thought to be essential for the crystallization process.[32] Therefore, the final temperature was set to 800 °C with a heating rate of 2.4 K min^{-1} in order to observe the crystallization for all three deposition methods adequately.

The results of the *in situ* annealing XRD are shown in Fig. 6. As expected there is a rapid crystallization around 300 °C within a few minutes for PLD grown films. However, the intensity drops as the annealing proceeds to higher temperatures. Similar to the *ex situ* annealed sample this effect can be attributed to micro-strain relaxation with increasing temperature as exemplified by a decrease in the FWHM of the XRD reflection peaks while the amplitude remains constant (not shown). Hence, it is important to note, that the integrated XRD intensity is not necessarily linearly dependent on the crystallized volume fraction as it was stated in ref. 22 and 50 where this assumption was used for powder samples. However, it can be assumed that the results shown for the isothermal dwells around 300 °C were not influenced by the micro-strain relaxation as the amount of stress should not have changed much during the measurements and no decrease of intensity with time was observed.

The sputtered film showed already a diffraction peak prior annealing, *i.e.* it was already partially crystallized during the room temperature deposition. An increase in the crystallized volume fraction was observed at ≈ 280 °C with a more gradual increase of the XRD peak intensity towards higher temperatures as compared to PLD grown films. The step-like increase around 280 °C is similar to the PLD grown samples which show a very sharp transition from amorphous to crystalline in a narrow temperature range at ≈ 300 °C. A ≈ 20 °C lower onset temperature

Published on 23 June 2015. Downloaded by MIT Library on 6/18/2019 3:35:39 PM.

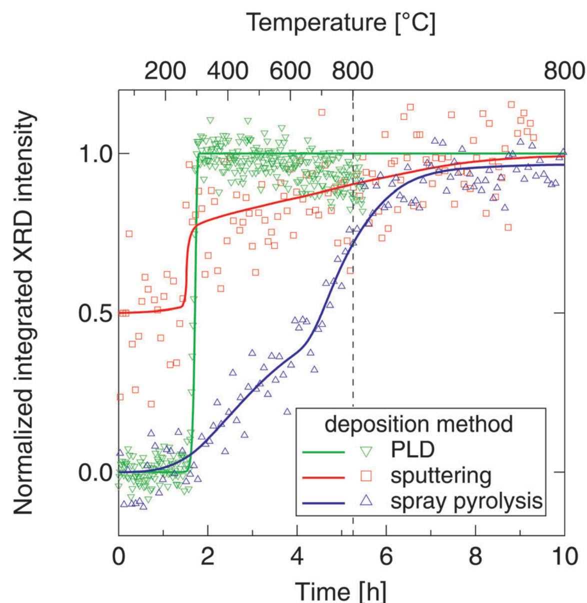

Fig. 6 Time evolution of the integrated XRD intensity of the (101) diffraction peak for YSZ thin films grown by PLD, SP and dc-magnetron sputtering. The heating rate was 2.4 K min^{-1} with a final temperature of 800 °C indicated by the dashed line. The solid lines are guides to the eye.

than for the PLD grown sample may be explained by an easier crystallization due to the already present crystalline phase (no nucleation necessary). The small increase also at higher temperatures is different to the observations for the PLD grown films. One possible explanation is that this increase encompasses also an at least partial recrystallization of the initially crystalline material, however, a detailed investigation has still to be performed, *e.g.* by TEM analysis of samples annealed at different temperatures.

For the SP grown sample a slow increase of crystallized volume fraction is observed with increasing temperature saturating after the final temperature of 800 °C was reached during three hours holding time. The onset of crystallization occurs already around 300 °C like for the other two samples. During the heating phase the crystallization rate increases two times, once around 400 °C and a second time just below 700 °C indicative for a two-step process. For a better illustration of these two regimes, the data points in the regions 2.5–4 h and 4–5.5 h were fitted to linear functions. The slopes were 0.10(3) h^{-1}, and 0.32(3) h^{-1}, respectively, clearly indicating an acceleration of the crystallization process. This result can be compared to the findings of Scherrer *et al.* who investigated the crystallization of SP grown YSZ thin films by scanning differential calorimetry (DSC) in combination with thermo gravimetry (TG).[32] They found an onset of crystallization above 370 °C accompanied by a mass loss, *i.e.* an oxidation and emission of organic residues from the precursor. Three exothermic maxima during the crystallization were determined in the DSC measurements. However, at a heating rate of 3 K min^{-1} two of them were close to each other around 730 °C and another in addition to that at 470 °C. This fits well with the present kinetic data of the SP films, where the second and third peak coincide with the fastest transformation rates, evaluated from the XRD intensity data.

Time–temperature-transformation diagrams for the amorphous to crystalline transition of PLD-YSZ thin films

In addition to the kinetics of the crystallization process, it is interesting to summarize the XRD crystallization data for the 3YSZ and the 8YSZ PLD grown thin films in time–temperature-transformation (TTT) diagrams, as shown in Fig. 7 (data for the latter films are taken from[22]). These TTT diagrams allow a simple and fast comparison of the crystallization process of different compositions, materials, and processing techniques.

The positions for 10%, 50% and 99% crystallized volume fraction were taken from the JMAK fitted curves of the temporal evolution of the diffraction peaks. At 10% the formation of nuclei is completed and the crystallization has already started whereas at 99% crystallization is essentially finished. As expected from the observation that the 3YSZ thin films did not crystallize at all at 250 °C, contrary to 8YSZ, the time needed to finish nucleation and the completion of crystallization took longer for the 3YSZ films at each investigated annealing temperature. Interestingly, this behaviour is different to findings on films deposited by a sol–gel method where a faster crystallization was observed for lower doped zirconia.[51]

A comparison of the generated TTT diagrams with other ceramic materials is difficult as not many studies are reported in literature. TTT diagrams for doped and undoped ceria thin films grown by SP can be found elsewhere.[28] Although different in chemistry this material has the same crystallographic structure as fully stabilized zirconia, *i.e.* cubic fluorite. Similar to the SP YSZ thin films of this study, the ceria SP thin films from[28] contained a large fraction of carbonyl and hydroxyl residues. These residues from the liquid precursor prevent rapid crystallization up to a temperature of ≈400 °C in both cases. In contrast,

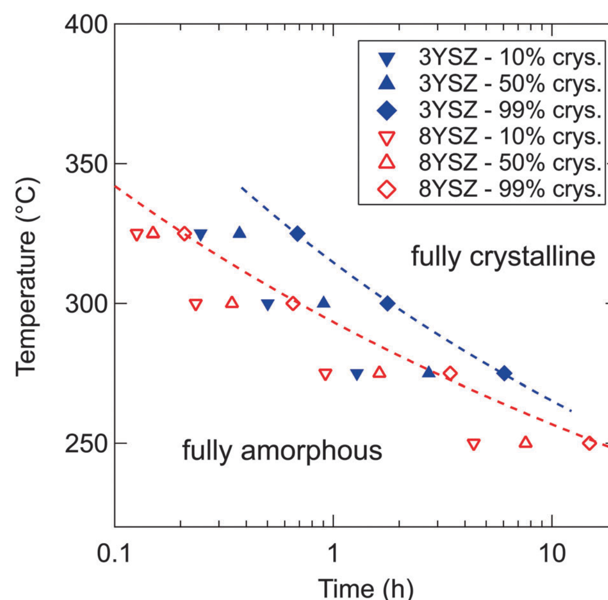

Fig. 7 TTT diagram for the 3YSZ (∇) and 8YSZ (Δ) [26] (4) PLD grown thin films. Indicated are the points, where 10%, 50% and 99% of the thin films were crystallized. The lines are guides to the eye and follow the 99% transformation point.

Published on 23 June 2015. Downloaded by MIT Library on 6/18/2019 3:35:39 PM.

the PLD-YSZ thin films without any residues from precursors crystallize already at 300 °C instantaneously to 100%. For the same degree of crystallinity the SP and dc-magnetron films have to be heated up to 1000 °C similar to the ceria thin films.[28] Furthermore, the PLD-YSZ thin films showed a strong reduction of crystallization time when the temperature was only a little higher than the minimum required for crystallization (factor of 3 for an increase of 25 K), while the SP-ceria thins films show this behavior only weakly (factor of 1.5 for an increase of 100 K).

Conclusions

Amorphous 3YSZ thin films were grown by PLD at ambient temperatures. Upon crystallization the films transform to a tetragonal zirconia phase with a ratio of $c/(\sqrt{2 \cdot a}) \approx 1$ for lower annealing temperatures up to 400 °C and increases for higher crystallization temperatures up to 1000 °C approaching a ratio of 1.014 indicative of an increased tetragonal distortion. The tetragonal phase was determined over the entire temperature range using Raman spectroscopy. A change from the t″ to the t′ phase takes place above 400 °C during crystallization.

Crystallization temperatures of 250 °C (3YSZ) and 275 °C (8YSZ) – reflecting the minimum temperature required to induce crystal growth of the nuclei in the films – were measured for PLD grown films. However, whether there is a direct relation between this relatively small difference in temperature and the doping concentration needs further investigation. From fits of the relative transformed volume with the JMAK model Avrami exponents around two for the 3YSZ, and three for 8YSZ thin films are obtained. These exponents may be attributed to the two growth modes, 2-, and 3-dimensional, respectively, which is also indicated by the morphology analysis by AFM, SEM, and TEM. While the 8YSZ thin films have average structure sizes similar to their film thickness of around 200 nm, the 3YSZ films showed lateral structure sizes around 1 μm and larger, resulting in high aspect ratios of 5–20. The crystallization measurements were also illustrated by time–temperature-transformation diagrams, which allow an easy comparison of the crystallization kinetics of YSZ thin films grown by PLD. 3YSZ thin films show a 1.5 times slower crystallization rate than 8YSZ thin films up to a temperature of 325 °C. Above this temperature the transformations of both compositions proceed faster than the time resolution of the XRD set-up. In constant heating rate experiments PLD grown films showed crystallization at around 300 °C within a few minutes. Thin films deposited by dc-magnetron sputtering were already partially crystallized during the deposition. Further crystallization sets in at around 300 °C, which is comparable to PLD grown films but the recrystallization kinetics was much slower and full recrystallization was only achieved at 800 °C. The SP grown samples showed the slowest onset of crystallization starting at ≈300 °C, but require for a full recrystallization more than 3 h at a final dwell temperature of 800 °C. Two different crystallization processes were identified at ≈470 °C and 730 °C, both coincide with exothermic maxima found in DSC measurements as reported previously.[32] This exemplifies the strong influence of organic residues on the crystallization properties and shows that the lowest thermal strain should be expected for PLD grown films since they fully recrystallize already at ≈300 °C, a temperature much lower than the targeted operating temperature of 400–500 °C for μSOFC.

Acknowledgements

This project is financed by the Paul Scherrer Institut and the Swiss National Science Foundation (SNF project No. 200021_126783). The Electron Microscopy ETH Zurich (EMEZ) is gratefully acknowledged for the use of their FIB and TEM facilities.

References

1 J. Maier, *Phys. Chem. Chem. Phys.*, 2009, **11**, 3011–3022.
2 G. Fadda, G. Zanzotto and L. Colombo, *Phys. Rev. B: Condens. Matter Mater. Phys.*, 2010, **82**, 064106.
3 H. L. Tuller, S. J. Litzelman and W. Jung, *Phys. Chem. Chem. Phys.*, 2009, **11**, 3023–3034.
4 H. Huang, M. Nakamura, P. Su, R. Fasching, Y. Saito and F. B. Prinz, *J. Electrochem. Soc.*, 2007, **154**, B20–B24.
5 A. Evans, A. Bieberle-Hütter, H. Galinski, J. Rupp, T. Ryll, B. Scherrer, R. Tölke and L. Gauckler, *Monatshefte für Chemie/Chemical Monthly*, 2009, **140**, 975–983.
6 A. Evans, A. Bieberle-Hütter, J. L. M. Rupp and L. J. Gauckler, *J. Power Sources*, 2009, **194**, 119–129.
7 I. Garbayo, A. Tarancón, J. Santiso, F. Peiró, E. Alarcón-LLadó, A. Cavallaro, I. Gràcia, C. Cané and N. Sabaté, *Solid State Ionics*, 2010, **181**, 322–331.
8 S. Rey-Mermet, Y. Yan, C. Sandu, G. Deng and P. Muralt, *Thin Solid Films*, 2010, **518**, 4743–4746.
9 D.-K. Lee, C. C. Fischer, I. Valov, J. Reinacher, A. Stork, M. Lerch and J. Janek, *Phys. Chem. Chem. Phys.*, 2011, **13**, 1239–1242.
10 C. Korte, J. Keppner, A. Peters, N. Schichtel, H. Aydin and J. Janek, *Phys. Chem. Chem. Phys.*, 2014, **16**, 24575–24591.
11 B. C. H. Steele and A. Heinzel, *Nature*, 2001, **414**, 345–362.
12 S. Presto, C. Information, A. Barbucci, M. P. Carpanese, M. Viviani and R. Marazza, *J. Appl. Electrochem.*, 2009, **39**, 2257–2264.
13 C.-W. Kwon, J.-W. Son, J.-H. Lee, H.-M. Kim, H.-W. Lee and K.-B. Kim, *Adv. Funct. Mater.*, 2011, **21**, 1154–1159.
14 J. L. M. Rupp, *Solid State Ionics*, 2012, **207**, 1–13.
15 A. Bieberle-Hütter, P. Reinhard, J. L. M. Rupp and L. J. Gauckler, *J. Power Sources*, 2011, **196**, 6070–6078.
16 M. Lugovy, V. Slyunyayev and R. Steinberger-Wilckens, *J. Power Sources*, 2009, **194**, 950–960.
17 T. Y. Koo, K.-B. Lee, Y.-H. Jeong and K. Y. Kang, *Jpn. J. Appl. Phys.*, 1998, **37**, 2629–2633.
18 T. Edler, J. Buschbeck, C. Mickel, S. Fähler and S. G. Mayr, *New J. Phys.*, 2008, **10**, 063007.
19 A. Evans, M. Prestat, R. Tölke, M. V. F. Schlupp, L. J. Gauckler, Y. Safa, T. Hocker, J. Courbat, D. Briand, N. F. de Rooij and D. Courty, *Fuel Cells*, 2012, **12**, 614–623.

Published on 23 June 2015. Downloaded by MIT Library on 6/18/2019 3:35:39 PM.

20 S. Heiroth, T. Lippert, A. Wokaun, M. Döbeli, J. L. M. Rupp, B. Scherrer and L. J. Gauckler, *J. Eur. Ceram. Soc.*, 2010, **30**, 489–495.
21 M. Gerstl, G. Friedbacher, F. Kubel, H. Hutter and J. Fleig, *Phys. Chem. Chem. Phys.*, 2013, **15**, 1097–1107.
22 S. Heiroth, R. Frison, J. L. M. Rupp, T. Lippert, E. J. B. Meier, E. Müller Gubler, M. Döbeli, K. Conder, A. Wokaun and L. J. Gauckler, *Solid State Ionics*, 2011, **191**, 12–23.
23 M. Ghatee, M. H. Shariat and J. T. S. Irvine, *Solid State Ionics*, 2009, **180**, 57–62.
24 S. Heiroth, J. Koch, T. Lippert, A. Wokaun, D. Günther, F. Garrelie and M. Guillermin, *J. Appl. Phys.*, 2010, **107**, 014908.
25 H. G. Scott, *J. Mater. Sci.*, 1975, **10**, 1527–1535.
26 C. H. Perry, F. Lu, D. W. Liu and B. Alzyab, *J. Raman Spectrosc.*, 1990, **21**, 577–584.
27 F. O. Adurodija, L. Semple and R. Brüning, *Thin Solid Films*, 2005, **492**, 153–157.
28 J. L. M. Rupp, B. Scherrer, N. Schäuble and L. J. Gauckler, *Adv. Funct. Mater.*, 2010, **20**, 2807–2814.
29 W. L. Bradley and R. Mattos, *Mater. Sci. Eng.*, 1975, **21**, 227–237.
30 W. L. Johnson, *Curr. Opin. Solid State Mater. Sci.*, 1996, **1**, 383–386.
31 J. F. Löffler, *Intermetallics*, 2003, **11**, 529–540.
32 B. Scherrer, S. Heiroth, R. Hafner, J. Martynczuk, A. Bieberle-Hütter, J. L. M. Rupp and L. J. Gauckler, *Adv. Funct. Mater.*, 2011, **21**, 3967–3975.
33 S. P. S. Porto and R. S. Krishnan, *J. Chem. Phys.*, 1967, **47**, 1009–1012.
34 I. Horcas, R. Fernandez, J. M. Gomez-Rodriguez, J. Colchero, J. Gomez-Herrero and A. M. Baro, *Rev. Sci. Instrum.*, 2007, **78**, 013705.
35 C. Suryanarayana and M. G. Norton, *X-ray Diffraction A Practical Approach*, Plenum Press, 1998.
36 P. Scherrer, *Nachrichten von der Gesellschaft der Wissenschaften zu Göttingen*, 1918, pp. 98–100.
37 M. A. Krivoglaz, *X-Ray and Neutron Diffraction in Non-ideal Crystals*, Springer-Verlag, Heidelberg, 1996.
38 E. Zolotoyabko, J. L. M. Rupp and L. J. Gauckler, *Scr. Mater.*, 2012, **66**, 190–193.
39 E. F. Lopez, V. S. Escribano, M. Panizza, M. M. Carnasciali and G. Busca, *J. Mater. Chem.*, 2001, **11**, 1891–1897.
40 M. Yashima, M. Kakihana and M. Yoshimura, *Solid State Ionics*, 1996, **86–88**, 1131–1149.
41 C. e. Viazzi, J.-P. Bonino, F. Ansart and A. Barnabé, *J. Alloys Compd.*, 2008, **452**, 377–383.
42 P. Bouvier and G. Lucazeau, *J. Phys. Chem. Solids*, 2000, **61**, 569–578.
43 P. Barberis, G. Corolleur-Thomas, R. Guinebretière, T. Merle-Mejean, A. Mirgorodsky and P. Quintard, *J. Nucl. Mater.*, 2001, **288**, 241–247.
44 M. Avrami, *J. Chem. Phys.*, 1939, **7**, 1103–1112.
45 W. A. Johnson and R. F. Mehl, *Trans. Am. Inst. Min. Metall. Eng.*, 1939, **135**, 416–441.
46 M. Avrami, *J. Chem. Phys.*, 1940, **8**, 212–224.
47 M. Avrami, *J. Chem. Phys.*, 1941, **9**, 177–184.
48 D. W. Henderson, *J. Therm. Anal. Calorim.*, 1979, **15**, 325–331.
49 S. L. dos Santos e Lucato, TU Darmstadt, FB Materials Science, Ceramics Group.
50 A. Ghosh, D. D. Upadhyaya and R. Prasad, *J. Am. Ceram. Soc.*, 2002, **85**, 2399–2403.
51 S. Ramanathan, R. V. Muraleedharan, S. K. Roy and P. K. K. Nayar, *J. Am. Ceram. Soc.*, 1995, **78**, 429–432.

 This journal is © the Owner Societies 2015